$Eu^{2+} \rightarrow Mn^{2+}$ energy transfer in NaCl

J. Rubio O. and H. Murrieta S.
Instituto de Física, Universidad Nacional Autonoma de Mexico, P.O.B. 20-364, Delagacion Alvaro Obregón, 01000 México, Distrito Federal, Mexico

R. C. Powell and W. A. Sibley
Physics Department, Oklahoma State University, Stillwater, Oklahoma 74078
(Received 8 June 1984)

Crystals of NaCl containing different concentrations of Eu^{2+} and Mn^{2+} ions (the Eu concentration always being less than that of Mn) were investigated by optical and EPR spectroscopy. The results show that Eu^{2+}-Mn^{2+} pairs form preferentially in this material and that highly efficient energy transfer occurs from the Eu^{2+} ions to the near-neighbor Mn^{2+} ions. Over 99% of the Eu^{2+} ions are paired, and these pairs are not significantly affected by the state of aggregation of the Mn ions, although in the various samples evidence for manganese ions in their dipolar state, as well as precipitated into the Suzuki phase, exists. The excitation spectra of the orange manganese emission show, in addition to the Eu^{2+} $4f^7 \rightarrow 4f^6 5d$ transitions, Mn^{2+} transitions associated with the Suzuki phase and with Mn^{2+}-cation vacancy dipoles. The peak positions of these Mn^{2+}-crystal-field-sensitive transitions were fitted theoretically with expressions including Racah-Tress and seniority corrections. This procedure allowed the determination of the relevant crystal-field parameters.

I. INTRODUCTION

As the utilization of optical devices becomes more prevalent in our society it is important to characterize the magnetic, electric, thermal, optical, and mechanical properties of transparent materials with divalent impurity ions in order to gain a more complete understanding of the physical processes and to develop more effective communication systems. A considerable advance has been made in the understanding of the optical properties of processes in alkali halide crystals doped with Eu^{2+} ions in the last few years.[1-7] It has been ascertained that Eu^{2+} ions give rise to two broad absorption bands in the ultraviolet region of the spectrum which are due to dipole-allowed transitions from the ground state $^8S_{7/2}$ of Eu^{2+} to the e_g and t_{2g} states of the excited $4f^6 5d$ configuration. The oscillator strengths of these transitions are around 10^{-2}, which makes these systems efficient absorbers of ultraviolet light. Moreover, the Eu^{2+} ions yield broadband emission (from $\sim$400 to $\sim$550 nm) when illuminated with radiation in either of the two uv absorption bands.

Since the optical properties of several divalent ions in the alkali halides[8-10] are fairly well understood, there is an increasing interest in the optical processes which involve more than a single-type ion in isolation. In particular, the investigation of radiationless transfer of optical excitation energy from one kind of optical center to another has received attention lately because of the importance of developing materials which can be used for laser and phosphor applications and for optical wavelength conversion.[11-20] For example, it is recognized that Mn^{2+} ions can be important phosphors but have the disadvantage that the $d \rightarrow d$ absorption transitions are difficult to pump since the transitions are strongly forbidden (oscillator strengths are of the order of 10^{-7}). However, excitation of the strong ultraviolet Eu^{2+} $f \rightarrow d$ transitions mentioned earlier, followed by energy transfer from Eu^{2+} as a donor, to Mn^{2+} as an acceptor, would provide an efficient mechanism for improving the efficiency of pumping the manganese ions. Therefore, in the present paper we report a detailed study of the NaCl:Eu,Mn crystal system using optical-absorption, photoluminescence, ionic thermocurrent (ITC), and electron paramagnetic resonance (EPR) techniques. This system presents the additional advantage that both ions can be measured in their dipolar state simultaneously by means of the ITC technique and independently with EPR. Measurements with these several different tools indicate that the Eu^{2+} and Mn^{2+} ions form pairs within the NaCl lattice that give rise to effective energy transfer and the promise of a very efficient device for optical conversion.

II. EXPERIMENTAL PROCEDURES

The single crystals of NaCl doped both with europium and with manganese were grown by R. Guerrero at the Institute of Physics of the National University of Mexico Crystal Growth Laboratory, using the Czochralski technique. In order to eliminate the presence of OH ions in the crystals an inert atmosphere of dry argon was maintained during the growing procedure. The dopants were $MnCl_2$ and $EuCl_2$, the latter being previously obtained from $EuCl_3 \cdot 6H_2O$ using standard reduction techniques. The concentration of the impurities in the crystals employed was determined by atomic absorption spectrophotometry. The Eu concentration was also calculated from the optical-absorption spectrum of the freshly quenched samples using the same procedure as described elsewhere.[4] The results obtained using both techniques were quite similar and did not differ by more than 15%. Thermal quenching was performed by heating the "as-grown" samples for 1 h at 550 °C and then dropping them onto either

a copper block or into acetone at room temperature.

Optical measurements were carried out with a Perkin Elmer 330 double-beam recording spectrophotometer. Excitation and emission spectra were obtained with a Perkin Elmer 650-10S spectro-fluorimeter, the excitation source being a 150-W xenon lamp. In all cases, the luminescence was observed at 90° to the direction of excitation. The wavelength resolution was ±2 nm. The excitation and emission spectra were corrected for lamp intensity and photomultiplier sensitivity, respectively.

Low-temperature measurements were taken with the crystals in either a CTI or an Air Products DE 202 cryogenerator which has a resistor heater for temperature control from 12 to 300 K.

In order to obtain a better understanding of the excitation and emission processes occurring in the doubly doped samples, the decay times of the orange manganese emission and of the blue europium luminescence were measured as a function of sample temperature. Lifetime measurements of the manganese emission were carried out by using a 75-W xenon lamp which was chopped at some desired frequency, a 0.22-m Spex excitation monochromator, a 0.8-m Spex emission monochromator, and a Biomation model No. 610B which was connected to a Nicolet 1070 signal averager. On the other hand, lifetime measurements of the Eu luminescence were made with a Molectron pulsed nitrogen laser, a 1-m Spex emission monochromator, and a boxcar integrator.

In order to determine the state of dispersion of both impurities in the crystals immediately after quenching, ionic thermocurrent measurements were also performed. A homemade cryostat evacuated to a pressure of 10^{-6} Torr or less in the temperature range 80—300 K was employed. The depolarization current was detected with a Keithley model No. 616 electrometer. This signal was then recorded versus temperature by a two-channel recorder. A chromel-alumel thermocouple embedded in a pure NaCl crystal was placed in the neighborhood of the sample in order to measure the sample temperature.

The electron paramagnetic resonance data were obtained using a conventional reflection-type *X*-band spectrometer with 100-KHz field modulation. A cylindrical cavity operating in the TE_{011} mode was employed. Crystal orientation was achieved by using a goniometer which allow rotation of the sample in two perpendicular planes.

III. EXPERIMENTAL RESULTS

The absorption of Eu^{2+} ions in a doubly doped crystal of NaCl containing 330 ppm of Mn^{2+} and 3 ppm of Eu^{2+} is illustrated in Fig. 1 for both as-grown and quenched samples. Although the oscillator strengths in the Eu^{2+}-ion transitions is about 10^{-2} and that of Mn^{2+}-ion transitions is only around 10^{-7}, it is possible to detect the Mn^{2+} absorption in relatively thick crystals. When NaCl:Eu,Mn crystals are illuminated with light having the appropriate wavelengths for absorption in the ultraviolet bands shown in Fig. 1, luminescence is observed. This emission is portrayed in Fig. 2 as a function of temperature. It should be noted that the 580-nm emission peak energy shifts to lower energy (longer wavelength) as

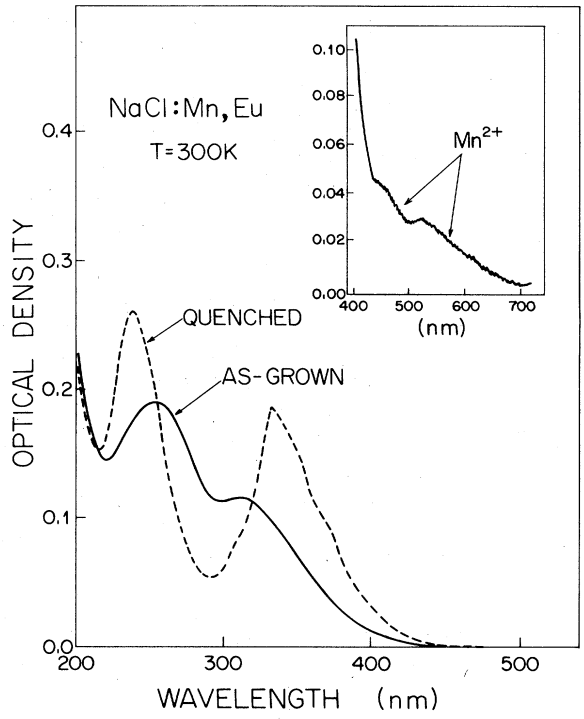

FIG. 1. Absorption spectra at 300 K for a NaCl:Mn,Eu containing 300 ppm Mn^{2+} and 3 ppm Eu^{2+} in as-grown and quenched samples. The sample thickness was 1.6 cm. The inset illustrates the weak Mn^{2+} absorption from 400 to 700 nm taken on a 8.3-cm crystal.

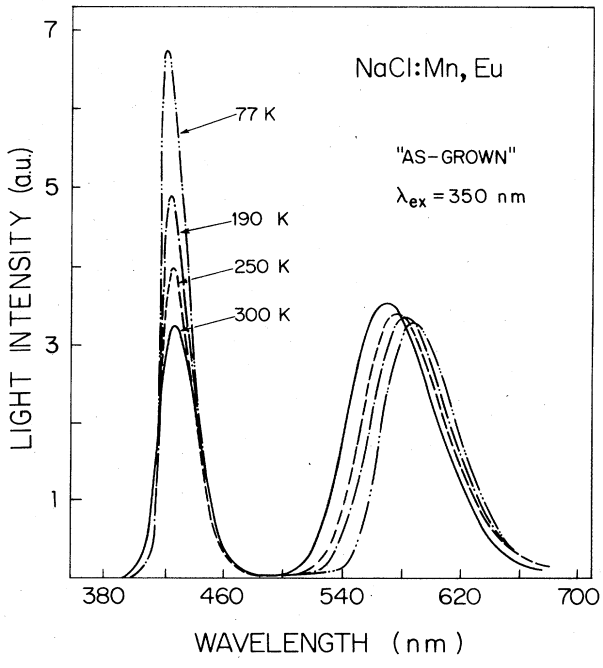

FIG. 2. Emission spectra for the same crystal used for the data in Fig. 1 as a function of temperature.

the temperature is lowered, whereas the 430-nm emission peak energy does not appreciably shift. Moreover, the area under this latter emission band remains the same for the temperatures measured. Both the peak energy and shift with temperature of the 580-nm band are consistent with Mn^{2+} emission characteristics. At room temperature in the as-grown sample used for Fig. 2 the Eu^{2+} emission and the Mn^{2+} emission have the same peak height intensity. A quench of this sample from high temperature results in an increase in the 430-nm emission as shown in Fig. 3. However, the 580-nm band remains constant even after rapid quenching in acetone. The same results were found in a crystal containing 100 ppm of Mn^{2+} and 20 ppm and Eu^{2+}, although after quenching a small increase ($\sim 15\%$) in the intensity of the 580-nm band was observed.

When emission from a crystal is observed it is possible to set the detecting monochromator at the peak energy of the emission and excite the sample with light from a second monochromator to determine those transitions that contribute to the emission. Since only those transitions which excite luminescence are detected, this is a much more powerful tool than absorption. Figure 4 shows the liquid-nitrogen excitation spectra for the emission observed at 580 nm. The intense excitation bands are those due to Eu^{2+} transitions, but even the weak Mn^{2+} bands can be observed. The room-temperature excitation data for the 430- and 580-nm bands in as-grown and quenched samples is illustrated in Fig. 5. The absorption and excitation data in Figs. 1, 4, and 5 in conjunction with atomic absorption impurity concentration determination make it possible to derive approximate oscillator strength values for some of the Eu and Mn transitions. These values are listed in Table I. Lifetime measurements were also performed on the emission transitions shown in Figs. 2 and 3. The results obtained are also summarized in Table I. The Mn^{2+} emission appeared as a pure exponential decay. The decay time increased continuously as temperature was lowered from 300 to 14 K, but show little change with thermal treatment of the sample. The Eu^{2+} fluorescence in a sample having no Mn^{2+} present also exhibited a pure exponential decay with only a slight shortening of the lifetime between the as-grown and quenched conditions. In the doubly doped crystals the Eu^{2+} decay patterns are more complex. Under as-grown conditions a nonexponen-

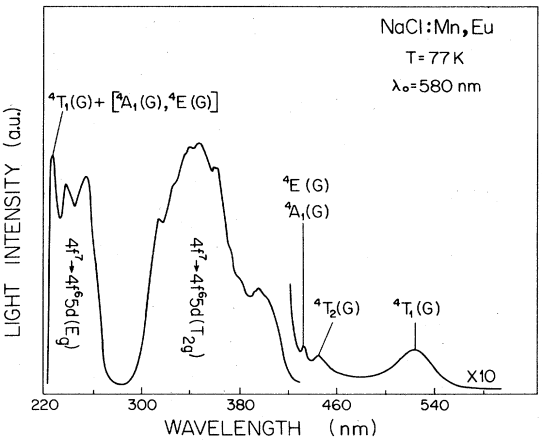

FIG. 4. Liquid-nitrogen excitation spectrum for the orange manganese emission. Assignment of some transitions are also included. The peak positions of other transitions and their assignment are given in Table II.

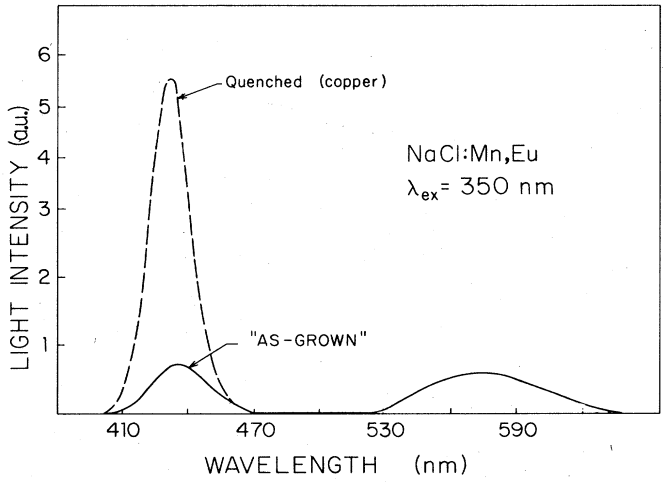

FIG. 3. Emission spectra at 300 K from the sample used for the data in Fig. 1 as in the as-grown and quenched conditions.

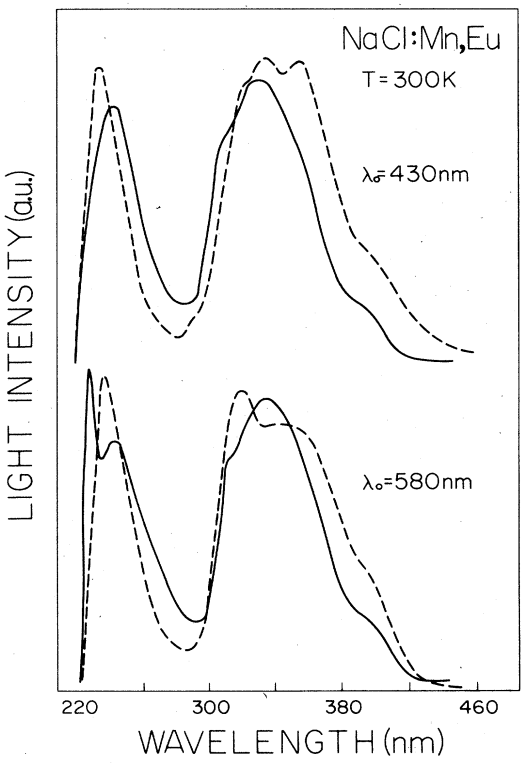

FIG. 5. Room-temperature excitation spectra for the Mn and Eu emission in as-grown and quenched samples. The spectra were taken on the same crystal used for the data in Fig. 1.

TABLE I. Fluorescence lifetimes and oscillator strengths of NaCl:Eu,Mn crystals. All data obtained at 300 K, except where indicated.

	Eu^{2+}		Mn^{2+}	
	Emission τ (sec^{-1})	Oscillator strength of the low-energy absorption band	Emission τ (sec^{-1})	Oscillator strength for the transition $^6A_1 \rightarrow {}^4T_1(G)$
NaCl:Eu (53 ppm)				
as-grown	2.76×10^{-7}			
quenched	2.16×10^{-7}	2.31×10^{-2}		
NaCl:Eu,Mn (30 ppm Eu; 200 ppm Mn)				
as-grown	$\sim1.30\times10^{-7}$[a]			
quenched (300 K)	2.54×10^{-7}[b]		2.45×10^{-2}	7.1×10^{-7}
(150 K)			3.72×10^{-2}	
(14 K)			4.74×10^{-2}	

[a] e^{-1} time for nonexponential decay.
[b] Double exponential decay.

tial decay is observed with a greatly reduced effective decay time. After quenching a double exponential pattern is observed with the initial decay time being close to that measured in the sample with no Mn^{2+} and the second decay time being much larger.

It is evident in Fig. 4 that at low temperatures there is considerable structure present in the excitation bands. From previous research it is well documented that various impurity phases exist in NaCl crystals doped with Mn^{2+} or Eu^{2+} and the absorption and emission of these impurity phases have been studied in detail.[5,21] The resolution of the data in Figs. 4 and 5 makes it possible to distinguish the transitions of these defects. This will be discussed in more detail later in the paper. For the reader's convenience the transitions energies of the fine-structure bands in the excitation spectra are provided in Tables II and III.

The emission data shown in Fig. 3 indicate that quenching a sample containing much less Eu than Mn results in a marked change in the 430-nm (Eu^{2+}) emission and no measurable change in the 580-nm (Mn^{2+}) emission. If the quenching process produces more Eu^{2+}-cation vacancy dipoles this should be evident in the EPR spectra. Figure 6(a) shows EPR measurements of an as-grown sample, and Fig. 6(b) illustrates the EPR spectrum after the sample has been quenched. It is evident that at least six times as many Eu^{2+} dipoles are detected, but it is

TABLE II. Positions of Eu^{2+} energy levels in NaCl:Eu at 77 K.

Eu^{2+} state ($4f^65d;T_{2g}$)	In isolated dipoles (nm)	Aggregates (nm)
$^7F_6$		317
$^7F_5$	340	332
$^7F_4$	354	345
$^7F_3$	364	354
$^7F_2$	375	368
$^7F_1$	382	382
$^7F_0$	392	397

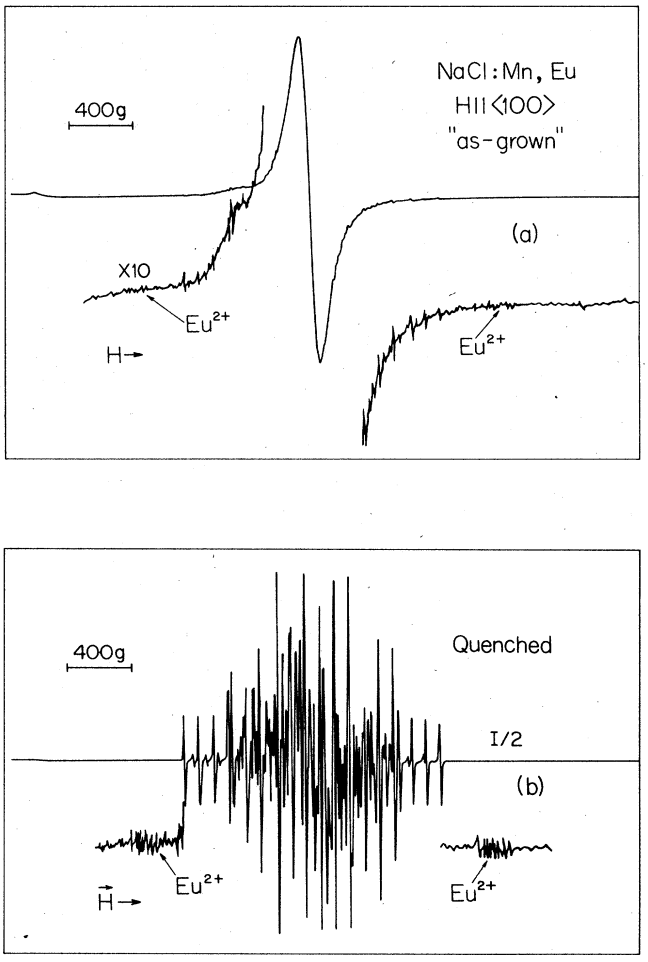

FIG. 6. Electron paramagnetic resonance spectra at 300 K for the sample used for the preceding figures: (a) before quenching, (b) after quenching. In this figure the letter *I* represents the amplifier gain used to record the spectra.

TABLE III. Position of Mn^{2+} energy levels in the doubly doped samples at 77 K.

Mn^{2+} state	Suzuki phase Observed (cm^{-1})	Suzuki phase Theory[a] (cm^{-1})	Dipoles Observed (cm^{-1})	Dipoles Theory[b] (cm^{-1})
$^4T_1(G)$	19011	18870	19380	19100
$^4T_2(G)$	22635	22771	23041	22894
$^4A_1$, $^4E(G)$	24044	23785	23923	23825
		23882		23917
$^4T_2(D)$	27285	27739	27510	27786
$^4E(D)$	28588	28598	28490	28634
$^4T_1(P)$	30257	30329	30395	30148
$^4T_2(F)$		37532		37696
$^4T_1(F)$		40225		40145
$^4T_2(F)$		41337		41184
$^4T_1(G)+[^4E(G),^4A_1(G)]$	434.78			

[a]Obtained using $Dq=625\ cm^{-1}$, $B'=840\ cm^{-1}$, and $\epsilon=0.038$.
[b]Obtained using $Dq=600\ cm^{-1}$, $B'=838\ cm^{-1}$, and $\epsilon=0.034$.

also evident that numerous Mn^{2+} dipoles have been produced by the quench even though there is no evidence of an emission increase for the 580-nm band in Fig. 3. At this point, it is important to point out that ITC measurements performed immediately after quenching revealed that not all the Mn ions were completely dispersed into the lattice. For example, for the crystal from which the data shown in Figs. 1—5 were taken, which contained 300 ppm Mn^{2+} ions and 3 ppm Eu^{2+}, only $\sim$150 ppm Mn^{2+}-cation vacancy dipoles were present after quenching. This fact indicates that Mn aggregates were present in these samples even after a severe quenching in acetone.

On the other hand, it is possible to follow the reduction of the Eu^{2+}- and Mn^{2+}-impurity dipoles as a function of the annealing time at 300 K after quenching. Figure 7 shows data taken by EPR and photoluminescence techniques. It might be noted that the crystals did not return to the original as-grown condition for times up to $\sim$100 h.

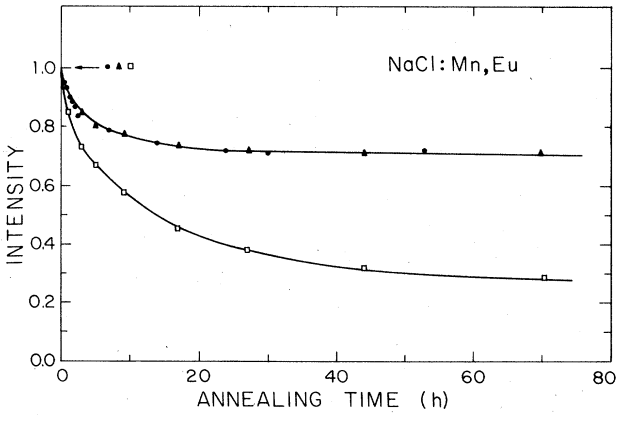

FIG. 7. Impurity-vacancy dipole decays in quenched NaCl:Mn,Eu as a function of annealing time at 300 K. The circles illustrate the decay of the Eu emission, the triangles the decay of the EPR Eu-signal intensity. The squares depict the decay of nearest-neighbor Mn^{2+}-cation vacancy dipoles as measured by EPR.

IV. DISCUSSION

The experimental results for NaCl crystals containing 300 ppm Mn^{2+} and 3 ppm Eu^{2+}; 200 ppm Mn^{2+} and 6 ppm Eu^{2+}; and 100 ppm Mn^{2+} and 20 ppm Eu^{2+} indicate that in all cases energy transfer occurs between Eu^{2+} ions and Mn^{2+} ions. This is most easily seen in Fig. 4, where it is apparent that Eu^{2+}-ion absorption produces Mn^{2+} emission. In addition, the quenching of the Eu^{2+} fluorescence lifetime due to the addition of Mn^{2+} in the as-grown samples (see Table I) can be attributed to energy transfer. The intensity of the Mn^{2+} emission is much greater than can be explained by energy transfer between statistically distributed impurity ions. In fact, for the low Eu^{2+} concentrations in these samples no effects of energy transfer would be observed if the impurity ions were distributed statistically.

For the complex system investigated here, it is not possible to unambiguously identify the nature of the ion-ion interaction producing the energy transfer. However, for qualitative comparisons of transfer properties for different sample conditions, it is useful to assume an electric dipole-dipole mechanism. The general arguments given below would also hold for higher-order multipole, magnetic, or exchange interactions. The expression for the electric dipole-dipole energy transfer rate is[22]

$$P_{dd}=\frac{3h^4c^4}{4\Pi n^4\tau_s}\left[\frac{1}{R_{sa}}\right]^6 Q_A \int \frac{f_s(E)F_A(E)}{E^4}dE\ , \qquad (1)$$

where τ_s is the radiative lifetime of the sensitizer ion, R_{sa} is the distance between the sensitizer and activator ions, and the integral represents the area of spectra overlap. Figure 8 illustrates the overlap between Eu^{2+} emission and Mn^{2+} absorption. The presence of significant overlap

suggests that efficient energy transfer is possible. However, when low impurity concentrations of only a few parts per million are present, R_{sa} is so large for statistically distributed impurities that $P_{dd} \approx 0$. The fact that energy transfer is observed in our samples implies that the impurities are not randomly distributed but rather occur as coupled pairs of Eu^{2+}-Mn^{2+}. A nearest-neighbor cation-cation separation distance in the NaCl lattice along the $\langle 100 \rangle$ direction for R_{sa} used in Eq. (1) predicts very efficient energy transfer.

This pairing might be expected in NaCl since Eu^{2+} has an ionic radius of 1.12 Å and Mn^{2+} and ionic radius of 0.8 Å. If these two ions couple through a Cl ion along a $\langle 100 \rangle$ direction, then they must fit into a space of 5.6 Å. Since Mn^{2+} is smaller than Na^+ ($R = 0.98$ Å) and Eu^{2+} is larger, the two ions together fit perfectly in the alloted space in the lattice.

The next question is, if the ions couple, how many of them are associated? Figures 2 and 3 show the relative intensities of Eu^{2+}-ion and Mn^{2+}-ion emissions. We assume as discussed above that for coupled Eu^{2+}-Mn^{2+} ions, the Eu^{2+} ions transfer their excitation energy efficiently to Mn^{2+} ions and do not contribute to the observed Eu^{2+} emission. Evidence supporting this assumption is gathered in Fig. 7, in which it is observed that the decay in concentration of Eu^{2+}-cation vacancy dipoles in the quenched sample as a function of the annealing time at room temperature as measured by EPR, correlates quite well with the decay in intensity of the Eu^{2+} emission peaking at 430 nm. This allows us to calculate the ratio of noncoupled Eu^{2+} ions ($N_{Eu^{2+}}$) to that of the coupled ions ($N_{Eu\text{-}Mn}$).

The intensity of the emission at a frequency ν is related to the number of excited ions N_e by[23]

$$I(\nu) = N_e P^r h\nu , \tag{2}$$

where P^r is the radiative rate of the transition. In our case, using the information in Table I and Figs. 2 and 3, we find

$$\frac{N_{Eu\text{-}Mn}}{N_{Eu}} = \frac{I_{Eu\text{-}Mn} P_{Eu} h\nu_{Eu}}{I_{Eu} P_{Eu\text{-}Mn} h\nu_{Mn}} \sim 10^5 . \tag{3}$$

Thus, over 99% of the Eu^{2+} ions are coupled to Mn^{2+} ions directly in this material. This fact might be suspected from the ionic radii argument made earlier and from previous investigations on the high mobility of Eu^{2+} ions in NaCl. However, this exceedingly high clustering probability may be verified from a careful study of the data. For example, if over 99% of the Eu^{2+} ions are associated with Mn^{2+} ions the absorption spectra shown in Fig. 1 must agree with the excitation data for Mn^{2+} emission portrayed in Fig. 4, since essentially all the absorption is due to Eu-Mn pairs. This agreement is evident from the figures. The change in absorption due to quenching can be explained as due to Mn-ion clusters around the Eu-Mn pairs being dispersed by the quenching. If this occurs, a small shift of the Mn^{2+} emission should be observed after quenching. Such an effect was found. In fact, low-temperature high-resolution data show that Mn^{2+} emission is slightly red-shifted after quench. The dispersion of Mn clusters is also evidenced by the increased Mn^{2+}-dipole concentration immediately after quenching (Fig. 6).

The fact that the fluorescence lifetime of the Eu^{2+} in the quenched sample is not decreased by the presence of the Mn^{2+} (see Table I) can be explained by assuming that all of the observed Eu^{2+} fluorescence under these conditions originates from ions not paired with a Mn^{2+} ion, whereas all of the paired Eu^{2+} ions transfer their energy so efficiently that they make no contribution to the observed fluorescence. The nonexponential decay pattern with a shortened lifetime for Eu^{2+} in the as-grown NaCl:Eu,Mn sample implies that the small number of Eu^{2+} ions which are not directly paired with Mn^{2+} ions are distributed at varying close separations from Mn^{2+} ions. One possibility for explaining this type of distribution is the presence of Eu^{2+} ions within a Suzuki-phase region of Mn^{2+} ions.[21] These regions are known to be present in about 10% of the as-grown crystal volume. The quenching treatment breaks up 90% of these regions as well as other impurity aggregates, and the observed Eu^{2+} emission is dominated by ions too far away from any Mn^{2+} ion to interact through energy transfer.

Previous work has illustrated the propensity for precipitates[2,3,21] and Suzuki phases[24–29] in this material. These defects and their effects can be seen in the data presented in this paper. Since precipitates, or even the Suzuki phase, take up only a small volume of the crystal the effects are small, but nonetheless observable. Figure 9 shows the emission for Mn^{2+} ions in the Suzuki phase ($\lambda_{ex} = 230$ nm) with no Eu^{2+} ions in the crystal (dashed line) and from Mn^{2+} ions in the doubly doped samples through direct excitation ($\lambda_{ex} = 520$ nm). The intensity of the Mn^{2+} emission and the energy of this emission peak when excited with $\lambda_{ex} = 360$ nm indicates energy transfer from Eu^{2+} to Mn^{2+} and a similar crystal field for Eu-Mn pairs and isolated Mn^{2+}. The presence of a band similar to the Suzuki-phase Mn^{2+} emission in these NaCl:Eu,Mn crystals suggests that the Suzuki phase of the Mn^{2+} ions

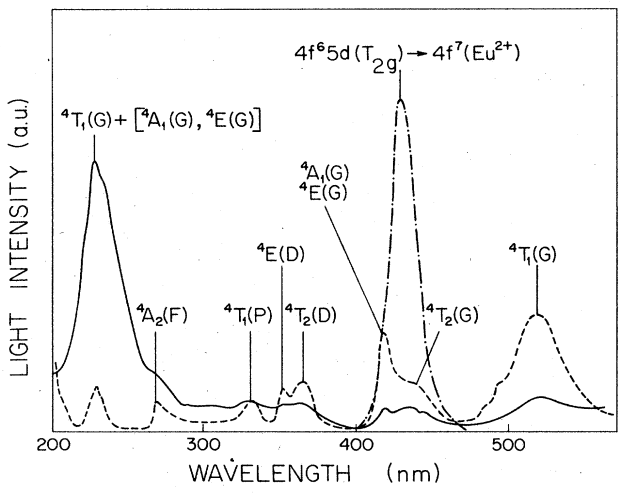

FIG. 8. Overlap region of the emission spectrum from Eu^{2+} and absorption spectrum of Mn^{2+} in NaCl at 300 K. The latter was taken from Rodríguez *et al.* (Ref. 21).

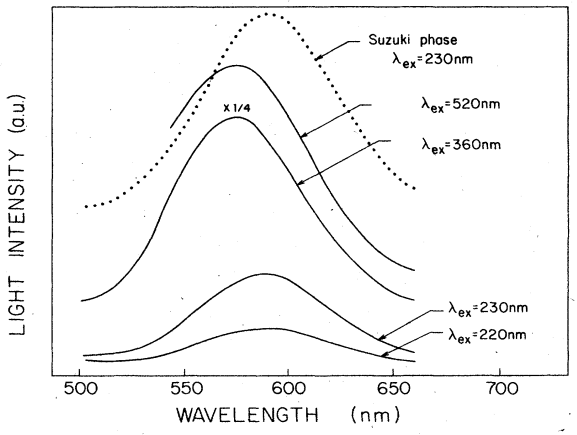

FIG. 9. Manganese emission spectra for various wavelengths of exciting light at 300 K in as-grown samples of NaCl:Mn,Eu. In the same figure, the emission spectrum of a NaCl:Mn sample in which the impurity is precipitated into the Suzuki phase is shown for comparison. The latter sample was kindly supplied by A. Gómez.

has been nucleated in the latter as-grown samples.

The structure appearing in the spectra can be explained through crystal-field considerations. The excitation spectra of the Mn-emission band taken in the as-grown samples and for a sample temperature in the range (12—77 K) show a complex structure due to the superposition of the Eu^{2+} and Mn^{2+} absorption transitions. As has been previously mentioned, in the as-grown samples there are several types of Eu-Mn and Mn-Mn defect complexes. Some of them are illustrated in Fig. 10. In the case of Eu-Mn pairs, it is expected that the crystal field acting on the europium ion should be mainly that of O_h symmetry as in the case of isolated Eu^{2+} ions, since the presence of a neighboring Mn^{2+} ion constitutes only a small perturbation to this crystal field. This can be verified by comparing the observed spectral structure obtained from the excitation spectra of NaCl:Eu with the number of transitions to ^7F_J levels predicted in O_h symmetry as listed in Table II. On the other hand, the orthorhombic crystal field due to the ⟨110⟩ charge compensating vacancy gives rise to a small crystal-field splitting of each J multiplet as has been discussed elsewhere.[1,30] The doubly doped samples present slightly broader transitions indicating that the interaction with the Mn^{2+} gives rise to only a small perturbation. Table II also lists the excitation peaks that appear in the low-energy band (T_{2g}) of the Eu^{2+} spectra for small aggregates. These peaks correlate quite well with some of those appearing in the doubly doped samples, which may then be due to an aggregate of Mn^{2+} ions in which the Eu-Mn pair has acted as a nucleation center (Fig. 10).

The other peaks appearing in the excitation spectra of the doubly doped as-grown samples are due to Mn^{2+} ions precipitated in the Suzuki phase. The presence of this second-phase precipitate was established through the observation of the 230-nm band in the excitation spectra of the Mn emission and ascribed to a double quantum transi-

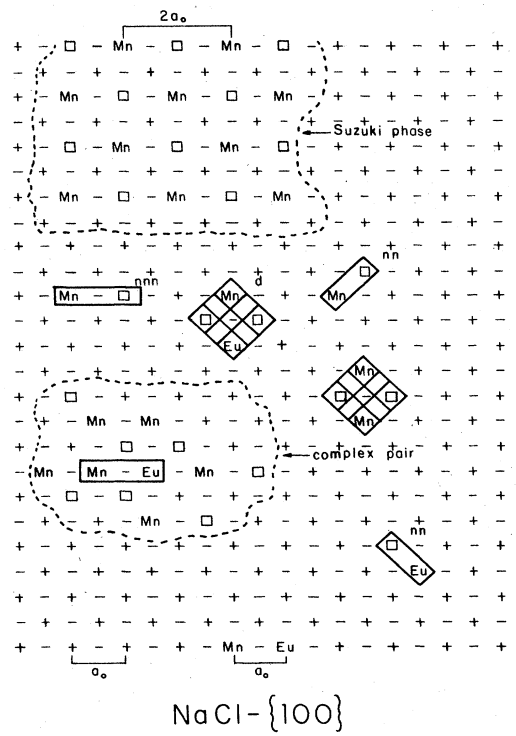

FIG. 10. Illustration of different impurity complexes in the alkali halide crystal doped with Eu^{2+} and Mn^{2+}.

tion $^6A_1 \rightarrow {}^4T_1(G)+[{}^4A_1(G), {}^4E(G)]$ as has been discussed by Rodríguez *et al.*[21]

In quenched crystals the overlap of the Eu^{2+} bands with those of the Mn^{2+} ions makes it difficult to measure precisely the Mn^{2+} peak positions. However, within experimental error, the measured peak positions in the doubly doped samples coincide with those reported by Rodríguez *et al.*[21] and are also similar to the as-grown case.

The Mn^{2+} crystal-field transitions have been fit using the procedure developed by Curie *et al.*[31] instead of the usual procedure of treating the Racah parameters B and C and the crystal-field splitting $10Dq$ as adjustable fitting parameters. The latter authors have shown that the inclusion of covalent effects as well as the Racah-Trees and seniority corrections provide better fits to Mn^{2+} data. In this procedure the adjustable parameters are Dq, a covalent reduced Racah parameter $B'(=BN_\tau^4)$, and the Koide-Pryce[32] covalency parameter ϵ. The results obtained using this procedure are shown in Table III for both Mn^{2+} ions in the dipolar state and the Suzuki phase. It should be noted that the effective $10Dq$ values found here are different from those obtained by Rodríguez *et al.*[21] This is due to the fact that Rodríguez *et al.*[21] used the Racah-Trees and seniority corrections in the weak-field scheme, whereas the energy-level structure of the Mn^{2+} ion was derived from the matrices obtained from the strong-field scheme in which these corrections are not diagonal. Using a similarity transformation, we have obtained the energy matrices in the strong-field

scheme, including the corrections mentioned above, following the procedure employed in Mehra.[33] The matrices are listed in the Appendix. The Racah-Trees and seniority corrections are specified by the parameters α and β, respectively, whose values were taken as in the free-ion case following Curie *et al.*[31] ($\alpha=65$ cm^{-1} and $\beta=-131$ cm^{-1}). The values obtained for B' and ϵ for Mn^{2+} into the Suzuki phase are quite similar to those obtained by Curie *et al.* for $MnCl_2\cdot 2H_2O$ ($B'=0.911$ and $\epsilon=0.024$). This result may suggest that in the Suzuki phase of the Mn^{2+} ions in the NaCl lattice, the Mn^{2+}-Cl^- distance is around 2.7 Å.

In summary, we have used optical and electron paramagnetic resonance spectroscopy to characterize the defect distributions in NaCl:Eu,Mn crystals having different thermal treatment histories. The most important conclusion drawn from the results of this work is the strong tendency for the Eu^{2+} and Mn^{2+} ions to form pairs in this host. The relative number of paired Eu^{2+} ions compared to impaired ions was found to be of the order of 10^5. Various sample conditions (i.e., as-grown, quenched, or annealed) produced easily observable changes in the details of the spectra as the percentage of impurity ions existing in different types of defect states such as dipoles, aggregates, Suzuki phases, etc. changed. However, under all conditions the great majority of Eu^{2+} ions exist in a paired state with Mn^{2+} and the thermally induced changes in the Mn^{2+} distribution produce only small perturbations on the Eu^{2+}-Mn^{2+} interaction. It may be suggested that in the "as-grown" samples several types of complexes as those shown in Fig. 10 are present, while in the quenched crystals, mainly Eu^{2+}-Mn^{2+} pairs, Mn^{2+}-cation vacancy dipoles as well as small Mn^{2+} aggregates (dimers, trimers, etc.) exist; the structure of the Mn^{2+}-Eu^{2+} pair being probably that of the dimer complex shown in the same figure. On the other hand, as the time after quenching proceeds, manganese ions aggregate to form bigger complexes. The data obtained may suggest that the Mn^{2+}-Eu^{2+} pair originally present after the quenching process, acts as a nucleation center for the manganese ions as illustrated in the complex pair depicted in Fig. 10. The impurity ion pairs exhibit extremely efficient energy transfer from Eu^{2+} to Mn^{2+}. Thus the strong tendency for pairing coupled with the efficient energy transfer provides a method for significantly increasing the Mn^{2+} luminescence by enhanced pumping through the Eu^{2+} ions. Finally, we may conclude that the NaCl:Eu,Mn is an excellent model system for demonstrating these effects which may prove useful in improving the efficiency of optical materials for various device applications. It is important to continue this line of investigation on other doubly doped crystal systems to determine the generality of the ionic radii criteria for producing the pairing effects.

ACKNOWLEDGMENTS

The authors are grateful to M. D. Shinn, G. E. Venikonas, R. López-Escalera, and J. Hernández A for their assistance with the experimental measurements. This cooperative research project was jointly sponsored by Consejo Nacional de Ciencia y Tecnología under Grant No. 237158 and by the National Science Foundation under Grant No. INT-81-20975.

APPENDIX

The energy matrices obtained by following the procedure employed by Mehra[33] are the following:

$$^4A_1(G)=27.825B'(1-\epsilon)+20\alpha\ ,$$

$$^4A_2(F)=16.695B'(1-\epsilon)+30.26B'(1-\epsilon)^2+12\alpha+2\beta\ ,$$

$$^4E(G,D)=\begin{bmatrix} 30.825B'-11.13B'\epsilon+14\alpha & 2\sqrt{3}B'(1-\epsilon)-4\sqrt{3}\alpha \\ 2\sqrt{3}B'(1-\epsilon)-4\sqrt{3}\alpha & 16.695B'(1-\epsilon)+15.13B'(1-\epsilon)^2+12\alpha \end{bmatrix},$$

$$^4T_1(G,P,F)=\begin{bmatrix} a & \alpha' & \beta_1 \\ \alpha' & b & \gamma_1 \\ \beta_1 & \gamma_1 & c \end{bmatrix},$$

$$a=17.825B'+5.565B'(1-\epsilon)+8B'(1-\epsilon)^2-10Dq+12\alpha+\tfrac{21}{85}\beta\ ,$$

$$b=32.825B'+11.13B'(1-\epsilon)+10\alpha+\tfrac{298}{85}\beta\ ,$$

$$c=10B'+7.13B'(1-\epsilon)+14.26B'(1-\epsilon)^2+A'\epsilon^2+10Dq+12\alpha+\tfrac{21}{85}\beta\ ,$$

$$A'=A\cdot\frac{B'}{B},\quad A=178\,400\ \text{cm}^{-1}$$

(from Lohr[34]), $B^*=918$ cm^{-1},

$$\alpha' = 3\sqrt{2}B'(1-\epsilon)^{1/2} + 2\sqrt{2}\alpha - \tfrac{58}{85}\sqrt{2}\beta ,$$

$$\beta_1 = 3.565B'(1-\epsilon) + 8\alpha + \tfrac{21}{85}\beta ,$$

$$\gamma_1 = 3\sqrt{2}B'(1-\epsilon)^{1/2} + 2\sqrt{2}\alpha - \tfrac{58}{85}\sqrt{2}\beta ,$$

$$^4T_2(G,D,F) = \begin{vmatrix} H & \alpha_2 & \beta_2 \\ \alpha_2 & P & \gamma_2 \\ \beta_2 & \gamma_2 & J \end{vmatrix} ,$$

$$H = 17.825B' + 13.565B'(1-\epsilon) + 8B'(1-\epsilon)^2 - 10Dq + 12\alpha + \beta ,$$

$$P = 19.695B' + 11.13B'(1-\epsilon) + 14\alpha ,$$

$$J = 10B' + 15.13B'(1-\epsilon) + 14.26B'(1-\epsilon)^2 + A'\epsilon^2 + 10Dq + 12\alpha + \beta ,$$

$$\alpha_2 = \sqrt{6}B'(1-\epsilon)^{1/2} - 2\sqrt{6}\alpha ,$$

$$\beta_2 = 7.565B'(1-\epsilon) + \beta ,$$

$$\gamma_2 = -\sqrt{6}B'(1-\epsilon)^{1/2} + 2\sqrt{6}\alpha .$$

[1] J. Hernández A., W. K. Cory, and J. Rubio O., J. Chem. Phys. **72**, 198 (1980).
[2] F. J. López, H. Murrieta S., J. Hernández A., and J. Rubio O., Phys. Rev. B **22**, 6428 (1980).
[3] J. Rubio O., H. Murrieta S., J. Hernández A., and F. J. López, Phys. Rev. B **24**, 4847 (1981).
[4] J. Hernández A., W. K. Cory, and J. Rubio O., Jpn. J. Appl. Phys. **18**, 533 (1979).
[5] H. Murrieta S., J. Hernández A., and J. Rubio O., KINAM **5**, 75 (1983).
[6] F. Jaque, J. Hernández A., H. Murrieta S., and J. Rubio O., J. Phys. Soc. Jpn. **51**, 249 (1982).
[7] J. Hernández, F. J. López, H. Murrieta S., and J. Rubio O., J. Phys. Soc. Jpn. **50**, 225 (1981).
[8] J. S. Dryden and R. G. Heydon, J. Phys. C **16**, 5363 (1983).
[9] C. Zaldo, J. Carcía Solé, and F. Agulló-López, J. Phys. Chem. Solids **43**, 837 (1982).
[10] C. Zaldo and F. Agulló-López, J. Phys. Chem. Solids **44**, 1099 (1983).
[11] F. Jaque, C. Zaldo, F. Cusso, and F. Agulló-López, Solid State Commun. **43**, 123 (1982).
[12] M. D. Shinn, J. C. Windscheif, D. K. Sardar, and W. A. Sibley, Phys. Rev. B **26**, 2371 (1982).
[13] D. K. Sardar, M. D. Shinn, and W. A. Sibley, Phys. Rev. B **26**, 2382 (1982).
[14] M. D. Shinn and W. A. Sibley, Phys. Rev. B **29**, 3834 (1984).
[15] Th. P. J. Borden, Philips Res. Rep. **7**, 197 (1952).
[16] T. L. Barry, J. Electrochem. Soc. **115**, 733 (1958).
[17] T. L. Barry, J. Electrochem. Soc. **117**, 381 (1970).
[18] M. Tamatani, Jpn. J. Appl. Phys. **13**, 950 (1974).
[19] A. L. N. Stevels and J. M. P. J. Verstegen, J. Lumin. **14**, 207 (1976).
[20] J. L. Sommerdijk and A. L. N. Stevels, Philips. Res. Rep. **37**, 221 (1977).
[21] F. Rodriguez, M. Moreno, F. Jaque, and F. J. López, J. Chem. Phys. **78**, 73 (1983).
[22] D. L. Dexter, J. Chem. Phys. **21**, 836 (1953).
[23] B. DiBartolo, *Optical Interactions in Solids* (Wiley, New York, 1968).
[24] K. Suzuki, J. Phys. Soc. Jpn. **16**, 67 (1961).
[25] J. A. Chapman and E. Lilley, J. Mater. Sci. **10**, 1154 (1975).
[26] E. Lilley and J. B. Newkirk, J. Mater. Sci. **2**, 567 (1967).
[27] W. Spengler and R. Kaiser, Status Solidi B **66**, 107 (1974).
[28] J. M. Calleja, A. Ruiz, F. Flores, V. R. Velasco, and E. Lilley, J. Phys. Chem. Solids **41**, 1367 (1980).
[29] F. Jaque, F. J. López, F. Cussó, F. Meseguer, and F. Agulló-López, Solid State Commun. **47**, 103 (1983).
[30] G. Aguilar S., E. Muñoz P., H. Murrieta S., L. A. Boatner, and R. W. Reynolds, J. Chem. Phys. **60**, 4665 (1974).
[31] D. Curie, C. Barthou, and B. Canny, J. Chem. Phys. **61**, 3048 (1974).
[32] S. Koide and M. H. L. Pryce, Philos. Mag. **3**, 607 (1958).
[33] A. K. Mehra, J. Chem. Phys. **48**, 4384 (1968).
[34] L. L. Lohr, J. Chem. Phys. **55**, 27 (1971).